Journal of Environmental Management 338 (2023) 117820

Contents lists available at ScienceDirect

Journal of Environmental Management

journal homepage: www.elsevier.com/locate/jenvman

Research article

Understanding the natural expansion of white mangrove (*Laguncularia racemosa*) in an ephemeral inlet based on geomorphological analysis and remote sensing data

Francisco Flores-de-Santiago [a,*], Ranulfo Rodríguez-Sobreyra [a], León Felipe Álvarez-Sánchez [b], Luis Valderrama-Landeros [c], Felipe Amezcua [d], Francisco Flores-Verdugo [d]

[a] *Instituto de Ciencias del Mar y Limnología, Unidad Académica Procesos Oceánicos y Costeros, Universidad Nacional Autónoma de México, A.P. 70-305, Av. Universidad 3000, Ciudad Universitaria, Coyoacán, Cd. México, 04510, Mexico*

[b] *Instituto de Ciencias del Mar y Limnología, Unidad de Informática Marina, Universidad Nacional Autónoma de México, A.P. 70-305, Av. Universidad 3000, Ciudad Universitaria, Coyoacán, Cd. México, 04510, Mexico*

[c] *Subcoordinación de Percepción Remota, Comisión Nacional Para el Conocimiento y Uso de la Biodiversidad, 4903 Liga Periférico-Insurgentes Sur, Tlalpan, Cd. México, 14010, Mexico*

[d] *Instituto de Ciencias del Mar y Limnología, Unidad Académica Mazatlán, Universidad Nacional Autónoma de México, Av. Joel Montes Camarena s/n, Mazatlán, Sin, 82040, Mexico*

ARTICLE INFO

Handling Editor: Jason Michael Evans

Keywords:
DJI Phantom
Google earth engine
Water level
Beach profile
Mexico

ABSTRACT

The interactions between local tides and river discharges are crucial in the processes related to the recruitment of mangrove propagules in estuarine systems. This investigation aimed to determine the causes of the recent natural recruitment and expansion of *Laguncularia racemosa* in mudflats within an ephemeral inlet in Mexico. We conducted a fluvial and coastal geomorphology assessment with spaceborne and UAV-based images. We deployed and recorded continuous data loggers in the estuarine system to assess water level and salinity. Depending on the available data, we used a combination of cloud-computing Google Earth Engine, UAV-Digital Surface Models, LiDAR, Google Earth images, and biophysical variables to monitor mangrove forests from 2005 to 2022. When the inlet is open, the estuarine system presents a full tidal range (∼1–1.5 m) with a strong salinity gradient (0–35 mS/cm), in contrast to the strong freshwater influence and minimal water level variability (<10 cm) that prevails for three months when the inlet is closed. Once the mouth of the river closes, there is considerable sediment accumulation, creating mudflat areas adjacent to the mangrove forests where *Laguncularia racemosa* propagules begin to establish under minimal water level variability and oligohaline conditions. After 16 years, the new forest expanded by 12.3 ha, presenting a very high density (10000 stems/ha), a considerable basal area (54–63 m^2/ha), and a maximum canopy height of 15.8 m, which largely surpasses that of other semiarid *Laguncularia racemosa* forests within permanent open-inlet systems or even in ephemeral inlets with different hydrological conditions. Our study will help to understand the causes of natural *Laguncularia racemosa* recruitment in extremely dynamic systems.

1. Introduction

Mangrove forests provide many ecosystem services, including nursery areas for endangered and commercial species (Muro-Torres et al., 2022), protection against storm surges and coastal erosion (Vizcaya-Martínez et al., 2022), and enhanced human development (Ferreira et al., 2022). Mangrove trees and shrubs thrive on mudflats, river banks, and coastlines in tropical and subtropical environments along the intertidal zone (Mafi-Gholami et al., 2020). They are the most capable of all aquatic and terrestrial ecosystems to store carbon (Pham et al., 2019; Blanco-Sacristán et al., 2022) and absorb dissolved nutrients (De-León-Herrera et al., 2015). Despite their ecological and economic relevance, mangrove ecosystems worldwide may be subject to constant degradation due to natural (e.g., hurricanes, sea-level rise, ocean temperature fluctuations) and anthropogenic (e.g., deforestation, pollution, urbanization, aquaculture) impacts (Arshad et al., 2020). For instance,

* Corresponding author.
E-mail address: ffloresd@cmarl.unam.mx (F. Flores-de-Santiago).

https://doi.org/10.1016/j.jenvman.2023.117820
Received 9 January 2023; Received in revised form 22 March 2023; Accepted 25 March 2023
Available online 30 March 2023

human repercussions accounted for 62% of the total mangrove area loss (3363 km^2) between 2000 and 2016 (Goldberg et al., 2020).

Although there are many studies about the possible causes of mangrove ecosystem degradation at a global scale (e.g., Schmitt and Duke, 2015; Flores-Verdugo et al., 2018; Kamal et al., 2021), very few recent studies have detected worldwide mangrove forest expansion in new areas (e.g., Flores-Verdugo et al., 2015; Chen et al., 2017; Mondal et al., 2018; Wang et al., 2021; Shih et al., 2022; Zhang et al., 2022). The ability of mangrove propagules to colonize new sites depends on recent hydrogeomorphic changes because these areas did not commonly have optimal conditions for mangrove development (Monroy-Torres et al., 2014). Results from field observations have suggested that sediment variability in the microtopographic profile, related to sediment dynamics, together with reductions in hydrodynamic forces, constitute the leading causes of early mangrove recruitment (Flores-de-Santiago et al., 2017; Shih et al., 2022). In this sense, while the hydrogeomorphic conditions are characteristic of coastal lagoon and estuarine environments, ephemeral inlets, where the connection to the ocean through the mouth of a river is not permanent, are unique systems because mangroves are under contrasting hydrosedimentary regimes (Godwyn-Paulson et al., 2021). For example, the temporal variability in water level, which quantifies the hydroperiod (frequency, duration, and intensity of flooding), together with the salinity of the system and water temperature, affects the spatial distribution of each mangrove species (Flores-Verdugo et al., 2018).

Accurate determination of mangrove extent due to natural expansion is not always straightforward (Nguyen et al., 2022); it implies extensive field studies, which can be labor-intensive and costly due to the inherent muddy environmental conditions in which mangroves grow (Field, 1998). In addition, historical analyses of biophysical data, such as forest structure, are usually unavailable for most places where mangrove expansion has occurred (Wang et al., 2018). Therefore, it appears that the only alternative for this endeavor is spatial data from remote sensing platforms (Guo et al., 2017). The relatively recent development of remote sensing technology has allowed the possibility of selecting a wide range of passive (multispectral) and active (LiDAR, radar) image datasets with spatial resolutions (pixel size) from sub-meter to tens of meters (Flores-de-Santiago et al., 2013; Tran et al., 2022; Lassalle et al., 2023). With the development of robust classification techniques (Lassalle et al., 2022), complex BigData processing application software, and cloud computing platforms, such as Google Earth Engine (GEE), the possibility of acquiring dense time series from remote sensing data has opened a new frontier in mangrove assessments, even at the species level (Vizcaya-Martínez et al., 2022). While global interest in the use of GEE in mangroves started in 2013 (Hansen et al., 2013), followed by case studies in Thailand (Pimple et al., 2018), Bangladesh (Mahmud et al., 2022), and China (Li et al., 2019; Zhang et al., 2022), only three recent studies have demonstrated the feasibility of GEE in Mexico (e.g., Valderrama-Landeros et al., 2021; Celis-Hernandez et al., 2022; Vizcaya-Martínez et al., 2022).

We hypothesized that the temporal variability between the continental water regime and the tides from the ocean controls the spatial geomorphology of the river mouth. If true, early white mangrove (*Laguncularia racemosa*) recruitment success will occur on recently created mudflats within the river when the flood regime presents minimal variability. We tested this hypothesis by evaluating the fluctuations of water level, coastal geomorphology of the river, and mangrove canopy area growth by means of several *in situ* and remote sensing approaches. The primary goal of this study was to evaluate historical trends in the natural expansion of *Laguncularia racemosa* in an estuarine system with an ephemeral inlet. Specifically, the objective of this study was fourfold. First, we assessed fluvial geomorphology changes throughout the river bank from the hydroelectric dam to the river mouth. Second, we analyzed the time series of water levels, salinity, temperature near the river mouth, and the height of the tides coming from the ocean. Third, we measured the coastal geomorphology complexity at the river mouth by means of remote sensing platforms. Finally, we quantify *Laguncularia racemosa* growth using a combination of historical remote sensing images, UAV flights, cloud computing time series, and a ground survey approach.

2. Materials and methods

2.1. Study area

The State of Sinaloa, located in the northwestern coastal region of Mexico, presents eleven main rivers that discharge into the southern entrance of the Gulf of California (Fig. 1a). The Sierra Madre Occidental Mountain range system (~3000 m amsl), which is part of the North American Cordillera, acts as a source of water in an otherwise arid/semiarid environment (Fig. 1b). The Presidio River rises in the high mountains and flows for ~170 km in a southwesterly direction across the state of Sinaloa until it reaches the coastal plain near the city of Mazatlan (Fig. 1c). Its catchment area is 5614 km^2, which causes an average annual discharge of 1779 hm m^3 (CONAGUA, 2015). Specifically, 76% of the drained volume occurs between June to October, being September the highest runoff (283 hm m^3). The climate near the river mouth is hot semiarid, causing an average annual air temperature of 24 °C, with monthly ranges from 21 °C in winter to 31 °C in summer (CONAGUA, 2019). The rainy season occurs during the summer (June to October), providing 78% of the total annual rainfall (500–1200 mm). There is additional lower rainfall (~35 mm) in winter (November to February) due to cold fronts from the upper Gulf of California. During the summer, extreme atmospheric events, such as tropical storms and hurricanes, may impact the study site (Vizcaya-Martínez et al., 2022).

The Presidio River is controlled by a dam (Picachos) which started operation in July 2009 (Fig. 1c). The dam is located at 75 m amsl and has a storage capacity of 328 hm m^3 within 2070 ha and a maximum depth of 50 m at the dam gate (Beltrá-Álvarez et al., 2012). The soil along the mouth of the Presidio River is of alluvial origin, with a high percentage of sand and silt recently deposited on the river bank. The dominant vegetation is low deciduous forests (<15 m height) and dense *Laguncularia racemosa* with a 16-m height (Fig. 1d). During the rainy season, the energy from the river breaks a sand bar at the mouth of the river (<200 m wide), exporting a massive amount of terrigenous material into the ocean. As river runoff decreases during the dry season, the ebb and flow of the tidal current and littoral transport tend to close the river inlet (CONAGUA, 2015).

2.2. Environmental data and mangrove field-based inventory

We collected field stem parameters of two mangrove plots where the natural expansion of *Laguncularia racemosa* occurred (Fig. 1d). We laid out two circular 0.012 ha plots as described by Kovacs et al. (2010) on February 22, 2022. Specifically, we determined the central location of each plot using a handheld Garmin GPSMAP 65s and recorded all stems of diameter at breast height (DBH) greater than 2.5 cm. We calculated stem density and basal area with the aforementioned data (Flores-Verdugo et al., 1987). The ideal way to determine the radius of the plot within the dense and muddy forest environment was using a waterproof distance meter STABILA Ld 420. We measured the height of the mangrove forest with a portable Vertex Laser VL400 hypsometer as described by Vizcaya-Martínez et al. (2022) and collected a series of photographs within the *Laguncularia racemosa* forest.

We installed a series of data loggers near the field survey transects and at a distance of ~800 m from the river mouth (Fig. 1d). Two initial Onset HOBO U20 instruments measured the river water level every 20 min for 278 days (11/20/2019 to 8/24/2020). Because of equipment loss (stolen), we could only install two new loggers eight months afterward that recorded water level data for 589 days (4/20/2021 to 12/1/2022). Although we were only able to install one Onset HOBO U24-002-C salt water conductivity (0.1–55 mS/cm) and temperature

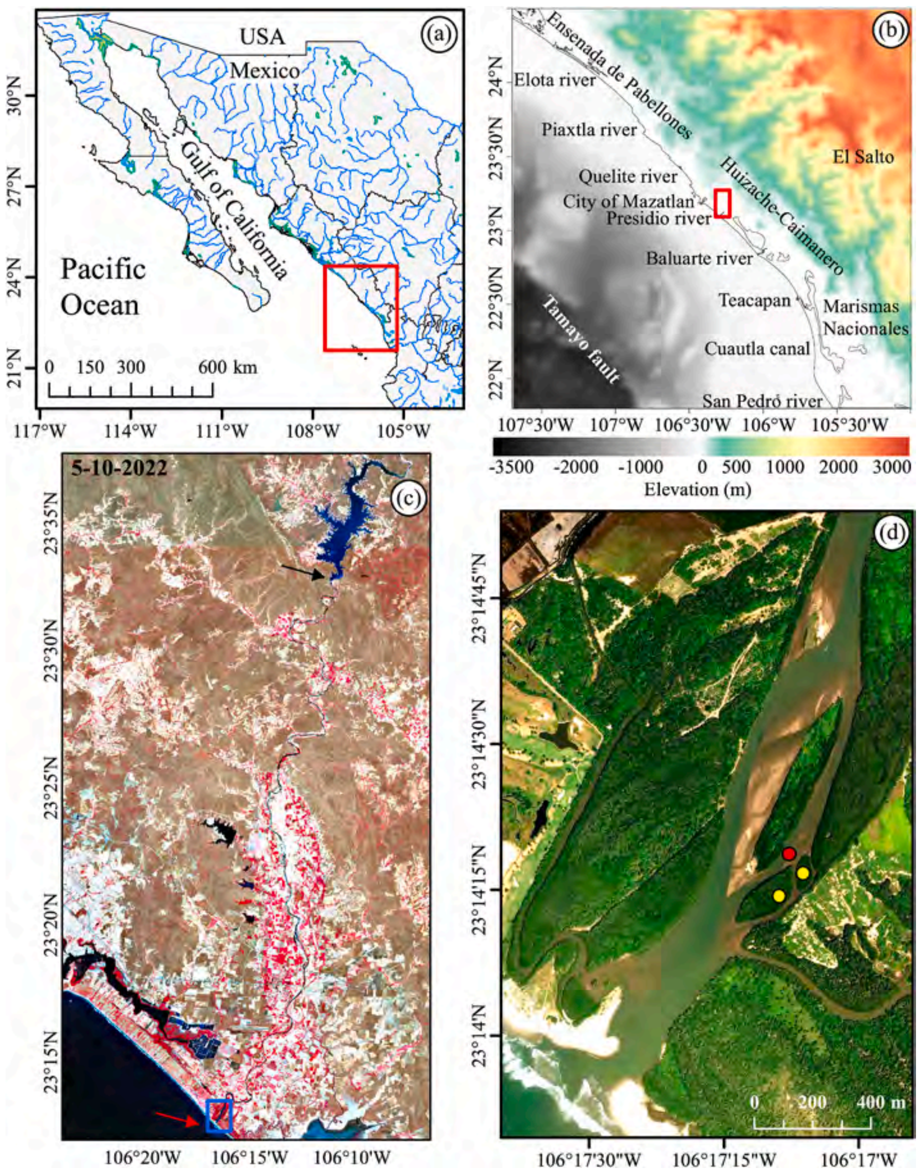

Fig. 1. (a) Hydrological system of the northwestern coast of Mexico (INEGI). The red rectangle indicates the border between the Sinaloa and Nayarit states. (b) Digital elevation model (m) of the east coast of the Gulf of California based on freely available TOPEX data (https://topex.ucsd.edu/cgi-bin/get_data.cgi). The red rectangle indicates the location of the Presidio River basin. (c) The coastal plain basin of the Presidio river between the Picachos reservoir and the Pacific Ocean (Enhanced Near-infrared, Red, Green of Sentinel-2 dated May 10, 2022). The black arrow indicates the Picacho's dam, and the red arrow the Presidio river inlet. (d) Visible Google Earth image of the white mangrove (*Laguncularia racemosa*) forests ecosystem along the Presidio river inlet. The red circle denotes the location of the HOBO water level logger. The yellow circles indicate the central position of the two mangrove field-based inventories.

(5–35 °C) logger for 90 days (5/9/2022 to 8/7/2022) due to budget constraints, the logger stopped recording data after the first deployment and required essential technical service. The underwater HOBO U20 measure absolute pressure (kPa), so they must be standardized according to atmospheric variability, so we recorded continuous atmospheric pressure with another HOBO U20 located on the roof of a nearby building, avoiding direct sunlight and rain. We determined the ocean's mean lower low water level (MLLWL) using the dominant lunar semidiurnal M2 tidal amplitude harmonic from freely available software downloaded at the Centro de Investigación Científica y de Educación Superior de Ensenada (http://predmar.cicese.mx). We extracted the time series of rainfall from NOAA (https://psl.noaa.gov/data/gridded/data.cpc.globalprecip.html) for the same time lapses recorded with the HOBO U20.

2.3. Remote sensing data collection and analysis

With a quick manual vectorization technique of the coastal plain river bank (~61 km long) on ArcMap software V.10.2.2 (Vizcaya-Martínez et al., 2022), we assessed the relatively recent (~18 years) geomorphological change detection through the Presidio River by means of freely available very-high spatial resolution Google Earth images (Nagarajan et al., 2022) from the last available date, prior to the construction of the Picachos dam (4/20/2003) and until the most recent image (3/29/2021). Regarding the recent mangrove expansion evaluation, we first detected the areas where this process occurred in the historical Google Earth dataset and verified the *Laguncularia racemosa* recruitment in the field. Subsequently, we selected all the available images from the beginning of the mangrove recruitment (March 8, 2005) until the most recent image. We used visual identification (Lassalle et al., 2022) and a vectorization technique to detect *Laguncularia racemosa*, according to Blanco-Sacristán et al. (2022), and calculated the increase in the canopy area (ha).

Selecting a representative location within the mangrove forest allowed us to understand the historical phenological trajectory of the naturally expanded *Laguncularia racemosa*. Due to the lack of high-resolution satellite images prior to 2005, we extracted the vegetation index NDVI, which is the most representative of abrupt mangrove forest phenology changes in this semiarid region (Vizcaya-Martínez et al., 2022) and other worldwide locations (Wang et al., 2018), by downloading individual bands (red and near-infrared) of the Landsat mission during the last 29 years (9/2/1992 to 6/2/2021). We analyzed the overall NDVI time series using the built-in GEE tool installed on the Quantum GIS V.3.16.13 software.

Regarding coastal geomorphology and the mangrove vertical structure, we acquired four seasonal sequences of UAV images at the Presidio River mouth in 2018 and 2019 and one fly mission over the mangrove forest in 2022, utilizing a rotary-wing DJI Phantom series quadcopter and its built-in visible camera, which is the most versatile UAV platform for coastal studies (Minervino Amodio et al., 2022). The UAV flight system captures individual images at the nadir view at 2 s intervals per image and stores the UAV location for each captured image in the flight log file (.csv) in the onboard internal measurement unit (IMU) and GPS. The autopilot software Map Pilot V.2.0.1 configured the flight missions over 30 ha and 10 ha for the Presidio River mouth and mangrove forest, respectively, following the approach described by Flores-de-Santiago et al. (2020).

Pre-flight white and black targets deployed at the control base station helped with the radiometric calibration of all individual images, as suggested by Flores-de-Santiago et al. (2020) and Dronova et al. (2021). We used Agisoft Metashape software V.1.5.2 (http://www.agisoft.com) to generate orthorectified images and digital surface models (DSM). Overall, the whole semiautomatic process involved three stages: (1) image alignment, (2) dense cloud construction, and (3) orthoimage/DSM generation. We traced a series of linear transects through the Presidio River sand barrier and the expanded *Laguncularia racemosa* forests and measured vertical profiles following the DSM approach described by Di Paola et al. (2022) and Vizcaya-Martínez et al. (2022). Additionally, we downloaded the only available airborne laser scanner (LiDAR) data (2012) from INEGI for historical upper canopy foliage comparisons, as suggested by Salum et al. (2020). We performed all the computer processing on a portable workstation, DELL Precision 7720, with Intel Core i7 processors (2.9 GHz), 64 GB of RAM, an NVIDIA Quadro P3000 6 GB graphic card, and 8 TB of storage divided into three

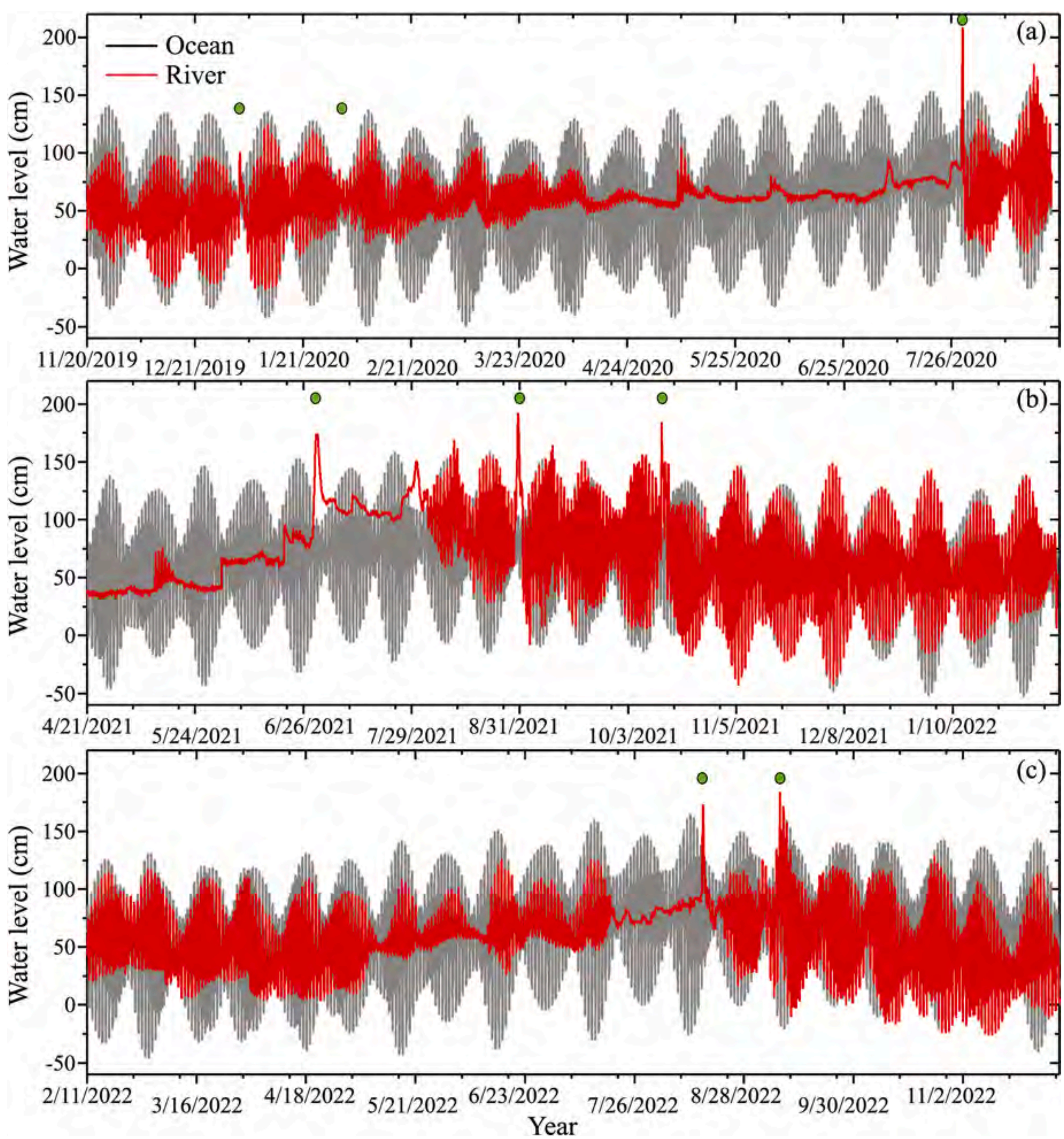

Fig. 2. Water level time series between the ocean (tidal harmonic) and the Presidio river inlet (HOBO U20). (a) The first nine-month period from November 20, 2019 to August 24, 2020. (b) and (c) The second 19-month period from April 20, 2021 to December 1, 2022. The green circles indicate the impact of major tropical storms and hurricanes.

Solid State Drives.

3. Results

The fluvial geomorphology of the Presidio River bank along the last 61 km of the coastal plain has had minimal variability in the last 18 years (Fig. S1a). Although both images represent dry season conditions (i.e., low water flow), there have been some geomorphic modifications, such as in the upper part close to the Picachos dam, as seen on the visible satellite comparisons (Fig. S1). However, the river's overall river bank and inlet do not present any apparent geomorphological change.

The water level of the Presidio River near the inlet presents the seasonal pattern expected for a river with an ephemeral sandbar. At the same time, the ocean tide shows typical behavior for this North Pacific coastline, with two daily high and low tides and a series of spring and neap tides every 15 days (Fig. 2). In the first time series of 278 days, the oscillation of the river water level was equivalent to the tide level coming from the ocean, but with a much lower intensity because the inlet of the river was not completely open. We detected punctual seasonal winter rainfall on January 3 and 22, 2020 (green dots). The river water level steadily decreased between February 2 and April 12, 2020. From April 12 to July 29, 2020, the river water level was practically stable, with water level changes of less than 10 cm because the inlet was fully closed. A hydrostatic head occurred between July 29 and 30 when the river water level increased to 125 cm in less than 12 h and caused the opening of the sandy barrier (green dot); consequently, the oscillation in the water level according to the ocean tide was once again appreciated (Fig. 2a).

In the second time series of 589 days, divided into two (Fig. 2 b and c), the river's water level was minimal because the mouth of the river was closed at the beginning of the time series on April 20, 2021. Another hydrostatic head appeared in July (green dot), but did not cause the inlet to open until August 2, 2021. The river water level presented abrupt increases of 175 cm and 170 cm during Hurricanes Nora (Aug 29–31, 2021) and Pamela (October 13, 2021), respectively (green dots). The river mouth opened at the beginning of November, represented by the onset of tidal oscillation (Fig. 2b). However, the inlet of the river began to close in December 2021, when there was a decrease in the river water level, until it closed completely on July 18, 2022 (Fig. 2c). Although the mouth of the river was semi-closed since December 2021, the water level began to decrease drastically from mid-May until it was completely closed on July 20, 2022. Following this process, the inlet of the river quickly reopened again on August 20 (green dot) during a heavy rain creating a hydrostatic head of 175 cm. In addition, a second hydrostatic head occurred at the beginning of September 2022 (green dot), which completely opened the inlet, reflecting an increase in tidal amplitude (Fig. 2c). The rainfall data from NOAA are similar to the river water level data. For example, the hydrostatic heads at the HOBOS water level coincide with the highest rainfall (Fig. S2).

Water salinity within the river depicts a transition between an open and closed inlet, which varied across the short 90-day time series (Fig. 3). When comparing the paired riverine water level and the salinity, we found a strong relationship between tidal force and river discharge at the river mouth. Water temperature within the river inlet fluctuated according to tidal amplitude and continued having a stable increase as the summer went by. For example, oligohaline conditions (0–2 mS/cm) and temperature (27 °C) appeared during neap tides when the river had full freshwater strength. On the contrary, salinity increases to full ocean water conditions (~35 mS/cm) during spring tides, and there was a natural fluctuation from 0 to 35 mS/cm that depended on the tidal amplitude. This pattern changed after the river inlet closure on July 18, when full oligohaline conditions prevailed because saltwater from the ocean could not enter the estuarine system directly.

The coastal geomorphology of the ephemeral inlet of the Presidio River shows a marked seasonal pattern. At the beginning of the opening of the inlet, the main river channel tends to present a direct connection with the ocean. As the dry season goes by and the discharge of the river decreases, the main channel begins to form a meandering configuration until the inlet closes, forming a perpendicular sandbar (Fig. 4). This seasonal pattern is annual, as observed in the UAV flights between 2018 and 2019, as well as in the two representatives Google Earth images in 2021. The river's water level is approximately 1 m above the mean sea level, as shown in the profiles extracted from the DSM of the UAV flights. The first coastal dune of around 3 m in height appears in the first 52 m-

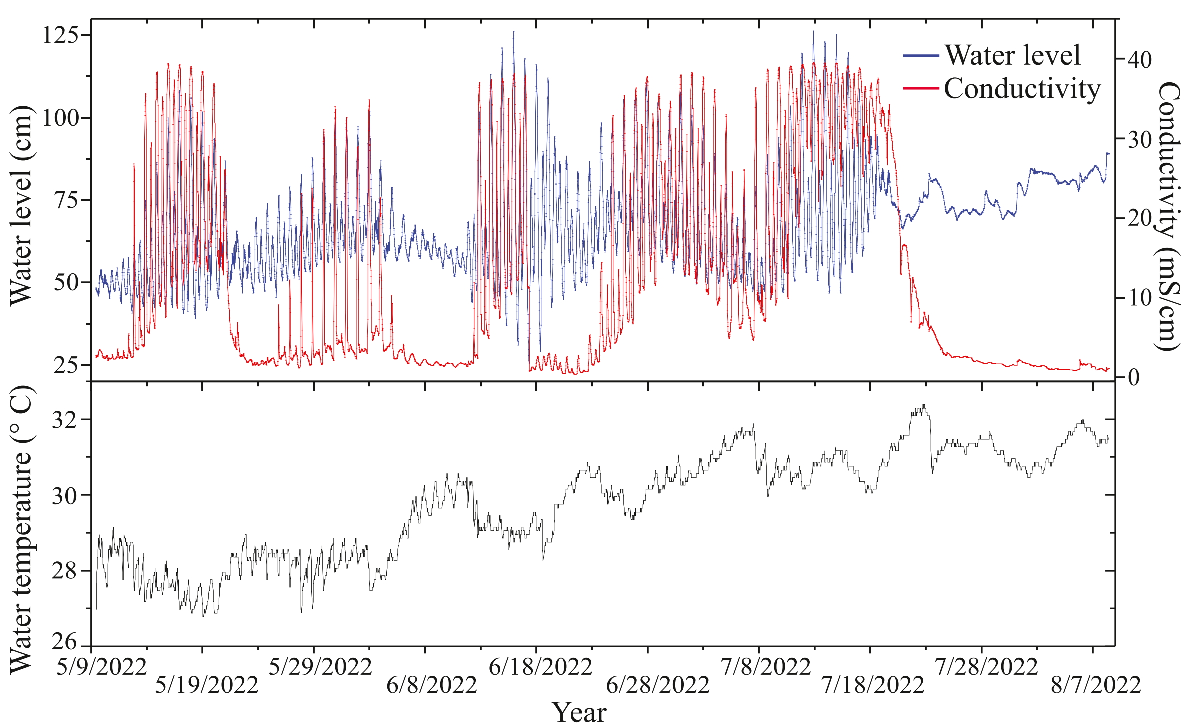

Fig. 3. Time series of water level, conductivity, and water temperature in the Presidio river inlet from May 9, 2022 to August 7, 2022.

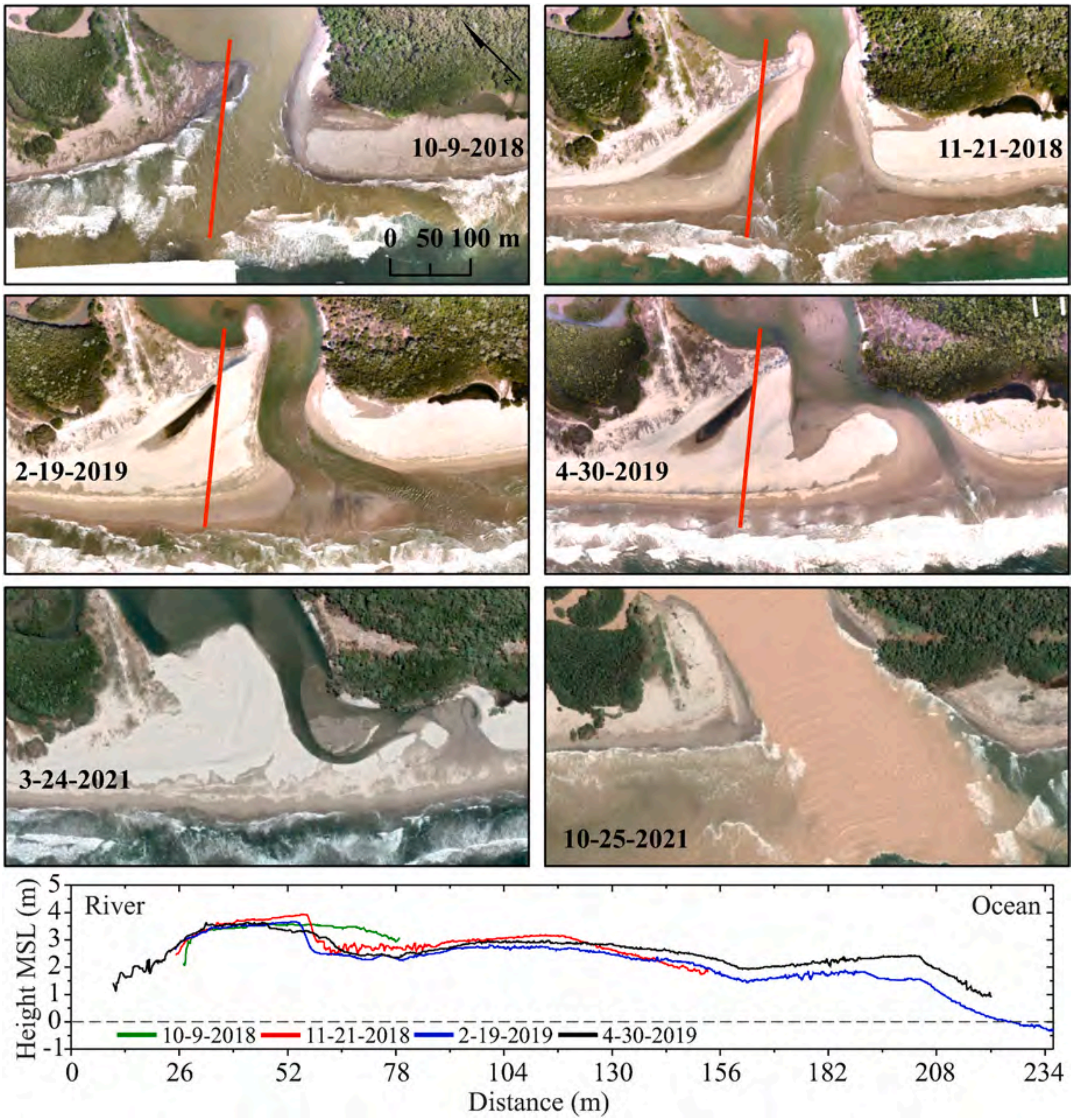

Fig. 4. Four orthomosaics from the UAV flights and two freely available Google Earth images depicting the coastal geomorphology variability of the ephemeral sandy bar. The red lines depict the 235-m path of the beach profile transects extracted from the UAV-DEM.

distance, followed by an extensive backshore of 2 m (~150 m), a berm (~40 m), and an abrupt beach slope. The most notable difference was seen in the berm zone between the DSMs of February and April 2019, where there was a 1-m high increase due to the accumulation of sedimentary material in two months (Fig. 4).

The expansion of *Laguncularia racemosa* in the area of the Presidio River inlet presents a different pattern between the two river banks. For example, growth in the western zone (right bank) does not occur along the main river bank, but rather in the sheltered areas behind the sandbar (Fig. 5a). In contrast, there has been a natural expansion along the river bank in the eastern zone (left bank), which is at approximately 800 m from the sandbar (Fig. 5b). The original area of the mangrove forest in 2005 was 23.7 ha and increased to 36 ha in 16 years. Considering a representative new mangrove forest area, the time series analysis of the NDVI vegetation index through the GEE platform indicates that the forest began to form between August 2005 and December 2007, depending on the area within the river. However, it was not until January 2017 that the mangrove forest canopy started to exhibit the classic phenological trend for subtropical mangroves, which is characterized by increases in the NDVI signal during the rainy season and decreases in the dry season (Fig. 5).

The vertical configuration of the mangrove forest varied along the river bank (Fig. 6). The DSM of the 2012 airborne LiDAR data shows a maximum tree height of 15–16 m at both edges of the river bank (Fig. 6a). Likewise, the orthomosaic and DSM of the 2022 UAV flights indicates a similar vertical configuration (Fig. 6b and c). Mangrove structure field data in this area show a maximum height of 15.8 m, using a digital hypsometer, which is very similar to that obtained by the LiDAR and UAV DSM data. Moreover, the stem density of both field plots was 10,345 stems/ha, and the basal area varied between 54 m^2/ha and 63.5 m^2/ha. The two vertical transects of 120 m in length throughout representative zones of natural expansion (T1 and T2) suggest that the LiDAR (2012) and UAV (2022) data show a different configuration that depends on the location of such transects because of the difference in data acquisition time. Both areas within the transects did not present mangrove seedlings before August 2005, indicating that the mangrove

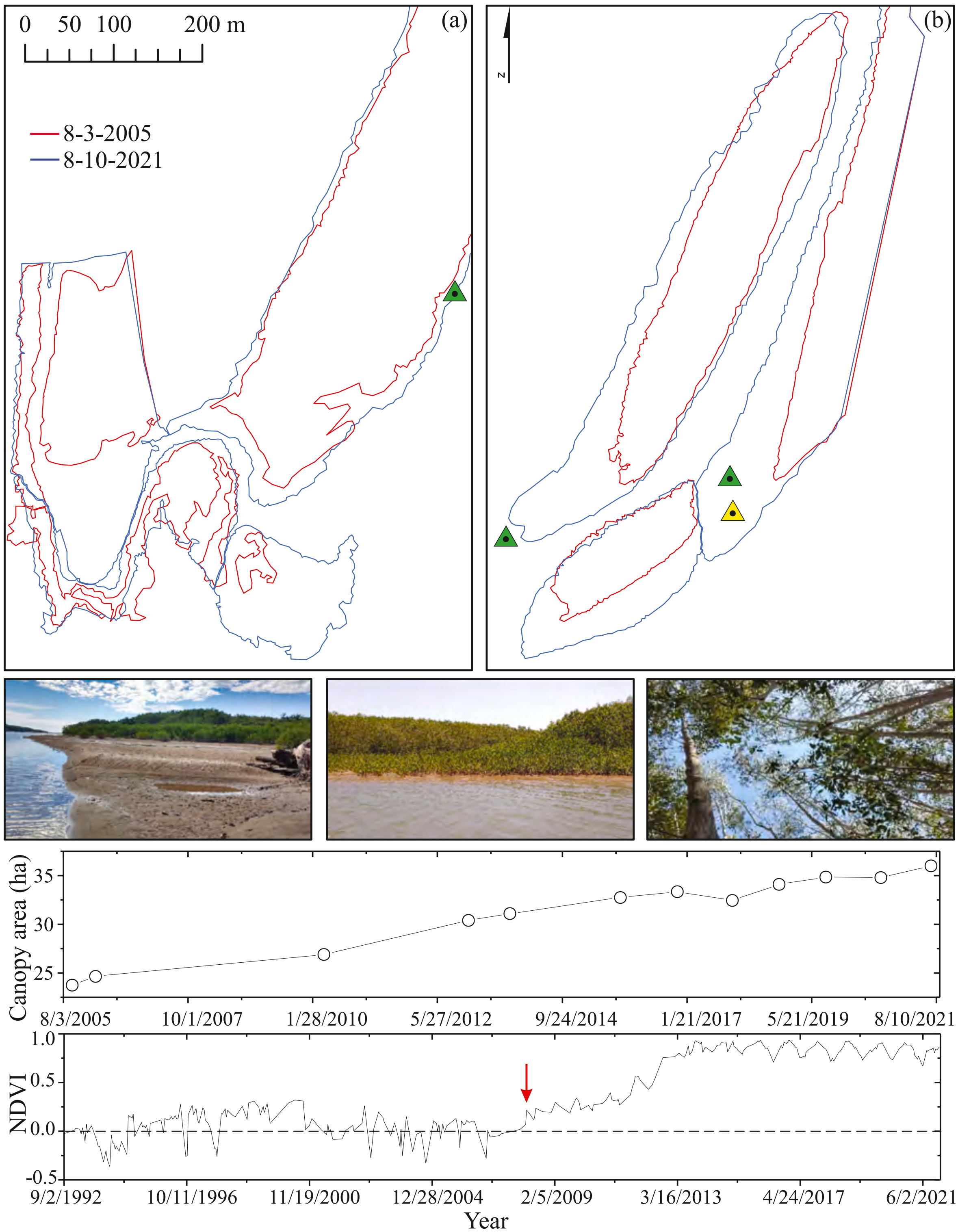

Fig. 5. Overall natural mangrove expansion (2005–2021) at the (a) right bank (West side) and (b) left bank (East side) of the Presidio river inlet. The green triangles depict the location of examples of field photos taken during low tide in August 2022. From left to right: tidal mudflats without *Laguncularia racemosa* seedlings, tidal mudflats colonized by *Laguncularia racemosa* seedlings, and a semi-hemispherical image of the expanded mangrove forest. The two graphs at the bottom depict the overall canopy area (ha) and the vegetation index (NDVI) time series extracted from the Google Earth Engine tool at the yellow triangle location.

forest began to expand in a southwesterly direction at T1. It is thus not surprising that the LiDAR data is similar to that of the UAV at the end of the transect (~110–120 m), given that this is the original mangrove forest which had established before the beginning of the time series. The evolution of the natural expansion in the vertical configuration of T1 is clear because there is a strong zonation between the young forest (<5 m) and the mature forest (~12 m). The T2 zone was initially an isolated mudflat area without vegetation; the mangrove seedlings started the natural recruitment process from the island's center. In this case, the recruitment was faster because the mangrove canopy showed the same height (~12 m) between both platforms, despite a 10-year difference. The recent seedling recruitment of *Laguncularia racemosa* was towards

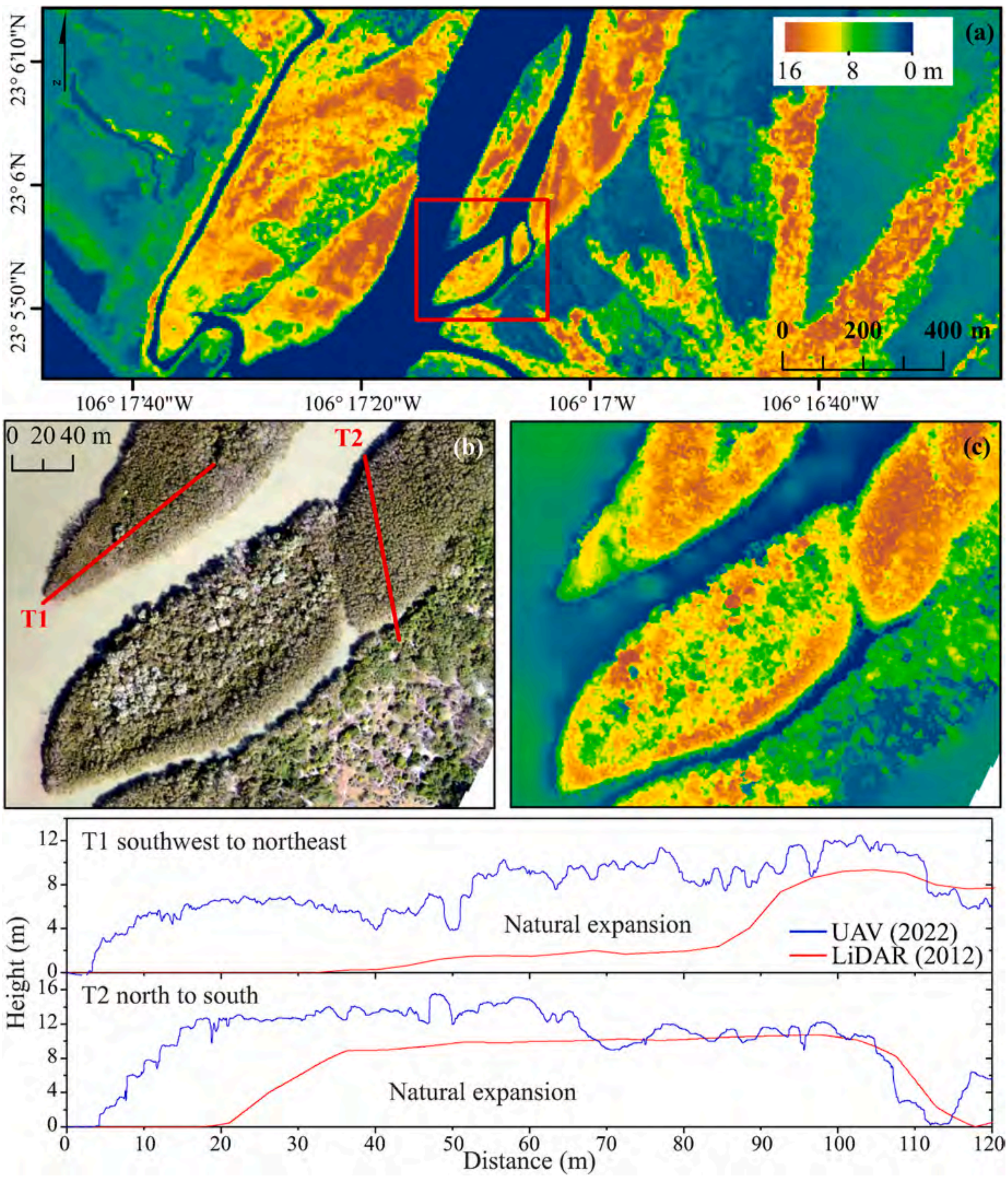

Fig. 6. (a) The only available LiDAR-DSM image of the study site. The red rectangle indicates the location of the UAV flight. (b) The orthomosaic (2.5 cm/pixel) and (c) the DSM from the UAV flights at a representative location where the mangrove expansion occurred. The red lines depict the path (120 m) of the two vertical transects (T1 and T2). The two graphs at the bottom depict the vertical configuration (LiDAR and UAV) of the two mangrove canopy transects throughout areas where no mangroves existed before 2005.

the north near the main channel where the sedimentation process was higher, enhancing the mangrove expansion, which was notable when comparing the vertical structure between the LiDAR data of 2012 (8 m) and those of the UAV of 2022 (12–13 m).

Based on the results, the hypothesis is accepted, showing that the spatial geomorphology of the river mouth depends on the interaction between the continental water and ocean tides. In addition, *Laguncularia racemosa* expansion occurs in areas adjacent to the forest under conditions where the flood regime presents minimal variability.

4. Discussion

Mangroves are ecologically complex ecosystems because their successful distribution depends on the species-specific hydro-sedimentary regime and the overall coastal geomorphology (Flores-Verdugo et al., 2018). In this sense, the combination of hydrological data (water level and salinity), freely available multispectral data from the GEE platform, and the spatial and vertical evolution of the mangrove forest through ultra-high spatial resolution orthomosaics/DSM from UAV were successful in analyzing and understanding the temporal, spatial, and vertical distribution of the *Laguncularia racemosa* canopy in previously unoccupied river bank mudflat areas.

The fluvial geomorphology of the Presidio River has not changed drastically in recent decades despite the construction of the Picachos dam. This situation may sound uncommon because anthropogenic activities, such as hydroelectric infrastructure, are known to change the natural sediment supply conditions, resulting in an overall degradation of mangrove habitats in the Mexican Pacific (Valderrama-Landeros et al., 2020) and at a global scale (Liang et al., 2023). For instance, the Santiago River, located at ~180 km southward, has shown massive beach erosion of 1.5 km and mangrove canopy loss of 334 ha since the construction of the Aguamilpa dam in 1993 (Valderrama-Landeros & Flores-de-Santiago, 2019). Another example is the Sinaloa River inlet, located at ~330 km northward, which has presented an overall beach erosion of 113 m (−3.1 m/year) during the last 37 years due to the construction of a hydroelectric dam and two breakwaters parallel to the inlet of the river (Zambrano-Medina et al., 2022). Contrarily, the contribution of sediments to the Presidio River could result from the extensive agricultural development along the river's lower basin (SAGARPA, 2018), which causes a constant supply of soil material through drained water and sediments from eroded soil that was once a natural deciduous forest. Another possibility could be the series of tributary streams between the Picachos dam and the mouth of the river throughout the 61 km that transports sediment to the coast. Unlike other semiarid rivers along the Sinaloa coast that dry up completely, the Presidio River always presents water that drains slowly, even in the dry season (CONAGUA, 2015). Additionally, the Picachos dam is relatively smaller (Beltrán-Álvarez et al., 2012) compared with other hydroelectric dams (Valderrama-Landeros and Flores-de-Santiago, 2019).

Laguncularia racemosa thrives in ephemeral inlet systems because it requires considerably less time for root establishment than other mangrove species, such as *Rhizophora mangle* and *Avicennia germinans* (Saenger, 2002; Flores-de-Santiago et al., 2017). Moreover, *Laguncularia racemosa* dominates in areas with a higher water level than the mean sea level (Flores-Verdugo et al., 1987), such as recently deposited sediments of runoff materials transported from upstream (Mafi-Gholami et al., 2020). In this case, the water level difference within the Presidio River inlet was 1 m above mean sea level when the inlet was closed because of the accumulation of freshwater from the river, which creates the ideal conditions for the early establishment of seedlings.

Based on the water level time series, there is an overall direct relationship between rainfall fluctuations and the water level within the *Laguncularia racemosa* forests. However, the latter depended on the ephemeral inlet variability. For example, there is a calm water condition in the *Laguncularia racemosa* forests between early March and the beginning of July, which creates suitable conditions for mangrove establishment. Nevertheless, the release time of the propagules of *Laguncularia racemosa* is from July to September (Benítez-Pardo et al., 2018), which coincides with the rainy season and the mouth of the river at its maximum opening. Hence, although we expected massive exportation of mangrove propagules to the ocean with the initial opening of the inlet, the remaining propagules trapped within the previously established mangrove seedlings would have found ideal conditions for early establishment once the inlet closed, creating zones of high accumulation of sediments through peat formation (Castillo et al., 2021). We expected the overall ephemeral inlet opening to vary through each of the rivers. For example, in the *Laguncularia racemosa* forests of the Quelite River, located at ~50 km northward, only 40% of the total litterfall is flushed into the ocean during the rainy season, and the mouth is open from July to September (Flores-Verdugo et al., 1987).

According to the conductivity profiles, the *Laguncularia racemosa* forests have received ample fresh water from the river despite being in a semiarid region, creating an oligohaline estuarine system once the inlet closes, which increases productivity, humic substances, and the capacity to store carbon (Flores-Verdugo et al., 1990; Flores-de-Santiago et al., 2012; Blanco-Sacristán et al., 2022). Sudden changes in salinity cause ecologically advantages for fauna, such as fish assemblages in the Presidio estuary (Muro-Torres et al., 2022); in addition, low salinity limits access to oceanic predators and increases the presence of typical estuarine and freshwater species absent in oceanic systems where the salinity is high. Thus, the fish assemblages are similar to those found in estuarine coastal waters, as in semiarid coastal lagoons (Amezcua et al., 2019). Therefore, the overall hydrological balance in the river inlet will change with the adverse effects of climate change alterations, such as the increase in droughts projected for arid and semiarid coasts (Mafi-Gholami et al., 2020).

The temporal variability of the opening of the Presidio River inlet depends on the river's water level, which must reach approximately a 1-m high hydrostatic head (water accumulation) for its inlet to open it. We do not know if this hydrostatic head is similar to other ephemeral river inlets because we have not found any published work about this. The overall geomorphology of the coast in front of the mouth of the Presidio River is very similar to the topographic beach profiles of southern Sinaloa; however, some differences have prevailed. For instance, the dune's height in areas adjacent to the mouth of the Presidio River oscillates between 6 and 8 m amsl (Valderrama-Landeros et al., 2022), which is higher than the 3.5 m extracted from the UAV-DSM. This pattern was foreseeable because the river inlet remains closed for only four months, and this does not allow the vertical deposition of enough sand (Serrano and Valle-Levinson, 2021). Although the advantages and disadvantages of UAV are well-known in the literature regarding coastal ecosystems (Dronova et al., 2021 and references therein), UAV data can complement freely available very high spatial resolution Google Earth images by providing vertical landscape composition.

Contrary to the vertical distribution of the beach sediment, the maximum cross-shore distance in front of the Presidio River mouth (208 m) is similar to the maximum beach distance (140 m) reported at 4 km to the north (Valderrama-Landeros et al., 2022). This pattern indicates that, once it closes, the inlet of the Presidio River stores a considerable amount of sediments which will flush into the ocean once the mouth opens (Vundavilli et al., 2021), thus creating accretion zones along the coastline. Consequently, the importance of the Presidio River for the coastal management of sandy beaches relies on its proximity with the entrance to the port of the city of Mazatlan at only 16 km northward from the mouth of the river, and this city has presented serious problems of coastal erosion due to unplanned developments (Valderrama-Landeros et al., 2022). Therefore, the conservation of the ecosystems near the Presidio River must be considered, given that there is a recent interest in developing the southern coastline of Sinaloa with seafront buildings.

The use of detailed Google Earth images to appreciate coastal changes is not new (Nagarajan et al., 2022), and one limitation is the lack of continuous data in remote locations. However, freely available multispectral data sources, such as the Sentinel-2 mission, could complement Google Earth images and benefit holistic assessments by helping with logistical surveying demands. Despite the fact that Google Earth images were not available before 2005 in this region, the NDVI time series shows that *Laguncularia racemosa* recruitment began between 2005 and 2007, depending on the river bank location. The growth of *Laguncularia racemosa* was greater than in environments without a freshwater source, such as semiarid coastal lagoons, which present salinities between 35 and 50 throughout the year (Flores-Verdugo et al., 2018). Many vegetation indices are available for mangrove ecology assessments; nevertheless, the NDVI has been the most widely used index (Baloloy et al., 2021; Tran et al., 2022) as it is the one that generates the best results in this type of semi-arid mangroves, detecting sudden canopy changes due to hurricane impact (Vizcaya-Martínez et al., 2022), comparisons multiple geomatic platforms (Valderrama-Landeros et al., 2018), and addressing phenological trajectories (Valderrama-Landeros et al., 2021). The errors that appeared in the NDVI time series before December 2007 could consist of variations in the water level detected at low tide (Kamal et al., 2016; Zhen et al., 2021; Mahmud et al., 2022) or were caused by the presence of seasonal patches of water lilies

(Flores-de-Santiago et al., 2016). Once the seedlings colonized the mudflats, the NDVI time series depicted a classic phenological trend for semiarid mangroves (Rioja-Nieto et al., 2017), where there is a marked oscillation between the rainy and dry seasons.

The national effort undertaken by the Comision Nacional para el Conocimiento y Uso de la Biodiversidad (CONABIO) to analyze accumulated anomalies in Sentinel-2 NDVI time series using GEE enabled the detection of the recent recruitment of *Laguncularia racemosa* propagules in at least five additional rivers along the Mexican Pacific coast from 2015 to 2020 (CONABIO, 2022). The increased spatial resolution of the Sentinel-2 data might have included mangrove stands that had not been previously identified using coarse spatial resolution data, such as Landsat (30 m) or MODIS (250 m) images (Blanco-Sacristán et al., 2022). Moreover, there are currently Sentinel-2-derived biophysical products that could be useful in identifying different mangrove zones despite the 10-m spatial resolution and are worth further study (Baloloy et al., 2021). In the future, it will be possible to use images of much higher spatial resolution at a low cost or even free to analyze mangroves in much greater detail (Lassalle et al., 2022; Tran et al., 2022). In the absence of hydrologic and UAV data, and given that the five-river systems vary in geomorphology, we intend to investigate each of them in detail. The expansion of *Laguncularia racemosa* in these fluvial systems presents a monospecific forest because, under these hydrosedimentary conditions, *Laguncularia racemosa* is capable of displacing other mangrove species (Monroy-Torres et al., 2014; Flores-de-Santiago et al., 2017), which depend more on tidal influence (*Rhizophora mangle*) and porewater salinity (*Avicennia germinans*) in semiarid coasts (Mafi-Gholami et al., 2020).

The structure of the recruited *Laguncularia racemosa* represents a highly dense forest (10000 stems/ha) with a high basal area (54–63 m^2/ha) and a 15.8-m height. It is completely different from the closest ephemeral inlet in the Quelite River, where the same mangrove species shows a much lower density (1430 stems/ha), basal area (12 m^2/ha), and height (7 m) (Flores-Verdugo et al., 1990). Unlike the Presidio River, the Quelite River has no constant freshwater supply. We had actually expected the mangroves to be under more stress in constant salinities of 30 due to only three months of freshwater input during the rainy season. Moreover, the structure of the Presidio River is also completely different from the closest coastal system without an ephemeral inlet (Urias system). This system is located 15 km northward, where the *Laguncularia racemosa* forest presents lower densities (6000 stems/ha), basal areas (30.8 m^2/ha), and height (6.2 m), characteristic of a system under the direct influence of the ocean (Valderrama-Landeros et al., 2021). These forest structure values are unsurprising, given that freshwater availability accounts for 74% of the global trends in the maximum canopy height and aboveground biomass values (Wang et al., 2019; Tran et al., 2022). Hence, detailed mangrove mapping and monitoring are of utmost importance to understand the geomorphic and environmental conditions that affect the composition of mangrove species and biophysical variables, such as leaf area, basal area, and canopy (Maurya et al., 2021).

5. Conclusions

Detailed maps of the distribution of both geomorphological and mangrove forests are needed so decision-makers may implement policy initiatives for the conservation of mangrove forests. We developed a comprehensive analysis to understand the natural recruitment of *Laguncularia racemosa* in an ephemeral inlet, combining *in situ* and remote sensing data. The variability in the time series of water level, salinity, and temperature indicates an alternation between oceanic and estuarine conditions depending on the geomorphology of the Presidio mouth. Once the river inlet closes during the dry season, the estuarine system presents ideal conditions for the recruitment of *Laguncularia racemosa* propagules, such as minimum water level fluctuation and an oligohaline water environment and thus accepting our hypothesis. Nevertheless, the current *Laguncularia racemosa* extent (12.3 ha with 15.8 m height) has provided the highest spatial resolution assessment of ephemeral inlets since 2005–something which would have proved to be impossible with traditional spaceborne platforms.

Unlike other rivers throughout Mexico's Pacific coast, the shoreline near the Presidio River mouth does not present major coastal erosion despite having a dam ~60 km upstream. Moreover, the recently expanded *Laguncularia racemosa* forest has shown unique biophysical variables, higher than mangroves within permanent open inlets or other ephemeral systems. Hence, its conservation is of utmost importance for sandy beach management. Considering that the recruitment of *Laguncularia racemosa* propagule was not uniform throughout the river bank, future work will include model simulations forced by river flow and quantification of suspended sediment export to the ocean.

Author statement

FFdS: Conceptualization, Data curation, writing review & editing, Funding acquisition. RRS: Data curation, Software. LFAS: Data curation, Software. LVL: Methodology, Software. FA: Validation, Supervision. FFV: Validation, Supervision, fieldwork, Funding acquisition. All authors read and approved the final manuscript.

Declaration of competing interest

The authors declare that they have no known competing financial interests or personal relationships that could have appeared to influence the work reported in this paper.

Data availability

Data will be made available on request.

Acknowledgment

Programa de Apoyo a Proyectos de Investigación e Inovación Tecnológica (PAPIIT-Mexico) provided funding for this investigation under Grants No. IA100218 and No. IA100521 awarded to FFdS. We are grateful for field assistance by Diego Vizcaya-Martínez and Roberto Cruz-García. Jazmín Corona-González processed the original version of the fluvial geomorphology data. Guillermina Feher edited the English text.

Appendix A. Supplementary data

Supplementary data to this article can be found online at https://doi.org/10.1016/j.jenvman.2023.117820.

References

Amezcua, F., Ramirez, M., Flores-Verdugo, F., 2019. Classification and comparison of five estuaries in the southeast Gulf of California based on environmental variables and fish assemblages. Bull. Mar. Sci. 95 (2), 139–159. https://doi.org/10.5343/bms.2018.0018.

Arshad, M., Eid, E.M., Hasan, M., 2020. Mangrove health along the hyper-arid southern Red Sea coast of Saudi Arabia. Environ. Monit. Assess. 192, 189. https://doi.org/10.1007/s10661-020-8140-6.

Baloloy, A.B., Blanco, A.C., Sharma, S., Nadaoka, K., 2021. Development of a rapid mangrove zonation mapping workflow using Sentinel 2-derived indices and biophysical dataset. Frontiers in Remote Sensing 2, 730238. https://doi.org/10.3389/frsen.2021.730238.

Beltrán-Álvarez, R., Ramírez-Lozano, J.P., Sánchez-Palacios, J., 2012. Temperature and dissolved oxygen of the Picahos reservoir, Sinaloa, Mexico. HIDROBIOLOGICA 22 (1), 94–98.

Benítez-Pardo, D., Benítez-Hernández, A., Flores-de-Santiago, F., Amador-Cruz, F., 2018. Phenology related nutrient content in leaves of *Laguncularia racemosa* (Combretaceae) in a tropical lagoon of the Gulf of California, Mexico. Acta Bot. Mex. 124, 227–234. https://doi.org/10.21829/abm124.2018.1326.

Blanco-Sacristán, J., Johansen, K., Duarte, C.M., Daffonchio, D., Hoteit, I., McCabe, M.F., 2022. Mangrove distribution and afforestation potential in the Red Sea. Sci. Total Environ. 843, 157098 https://doi.org/10.1016/j.scitotenv.2022.157098.

Castillo, Y.B., Kim, K., Kim, H.S., 2021. Thirty-two years of mangrove forest land cover change in Parita Bay, Panama. For. Sci. Technol. 17 (2), 67–79. https://doi.org/10.1080/21580103.2021.1922512.

Celis-Hernandez, O., Villoslada-Peciña, M., Ward, R.D., Bergamo, T.F., Perez-Ceballos, R., Girón-García, M.P., 2022. Impacts of environmental pollution on mangrove phenology: combining remotely sensed data and generalized additive models. Sci. Total Environ. 810, 152309 https://doi.org/10.1016/j.scitotenv.2021.152309.

Chen, B., Xiao, X., Li, X., Pan, L., Doughty, R., Ma, J., Dong, J., Qin, Y., Zhao, B., Wu, Z., Sun, R., Lan, G., Xie, G., Clinton, N., Giri, C., 2017. A mangrove forest map of China in 2015: analysis of time series Landsat 7/8 and Sentinel-1A imagery in Google Earth Engine cloud computing platform. ISPRS J. Photogrammetry Remote Sens. 131, 104–120. https://doi.org/10.1016/j.isprsjprs.2017.07.011.

CONABIO (Comisión Nacional para el Conocimiento y Uso de la Biodiversidad), 2022. http://geoportal.conabio.gob.mx/metadatos/doc/html/rm_pn1520gw.html.

CONAGUA (Comisión Nacional del Agua), 2019. Estadística del agua en México. Ciudad de México, p. 276.

CONAGUA (Comisión Nacional del Agua), 2015. Actualización de la disponibilidad media anual de agua en el acuífero Río Presidio (2509). Estado de Sinaloa. Ciudad de México, p. 37.

De-León-Herrera, R., Flores-Verdugo, F., Flores-de-Santiago, F., González-Farías, F., 2015. Nutrient removal in a closed silvofishery system using three mangrove species (*Avicennia germinans, Laguncularia racemosa*, and *Rhizophora mangle*). Mar. Pollut. Bull. 91, 243–248. https://doi.org/10.1016/j.marpolbul.2014.11.040.

Di Paola, G., Minervino Amodio, A., Dilauro, G., Rodriguez, G., Rosskopf, C.M., 2022. Shoreline evolution and erosion vulnerability assessment along the central Adriatic coast with the contribution of UAV beach monitoring. Geosciences 12, 353. https://doi.org/10.3390/geosciences12100353.

Dronova, I., Kislik, C., Dinh, Z., Kelly, M., 2021. A review of unoccupied aerial vehicle use in wetland applications: emerging opportunities in approach, technology, and data. Drones 5, 45. https://doi.org/10.3390/drones5020045.

Ferreira, A.C., Borges, R., de Lacerda, L.D., 2022. Can sustainable development save mangroves? Sustainability 14, 1263. https://doi.org/10.3390/su14031263.

Field, C., 1998. Rationales and practices of mangrove afforestation. Mar. Freshw. Res. 49, 353–358. https://doi.org/10.1071/MF97127.

Flores-de-Santiago, F., Valderrama-Landeros, L., Rodríguez-Sobreyra, R., Flores-Verdugo, F., 2020. Assessing the effect of flight altitude and overlap on orthoimage generation for UAV estimates of coastal wetlands. J. Coast Conserv. 24, 35. https://doi.org/10.1007/s11852-020-00753-9.

Flores-de-Santiago, F., Serrano, D., Flores-Verdugo, F., Monroy-Torres, M., 2017. Application of a simple and effective method for mangrove afforestation in semiarid regions combining nonlinear models and constructed platforms. Ecol. Eng. 103, 244–255. https://doi.org/10.1016/j.ecoleng.2017.04.008.

Flores-de-Santiago, F., Kovacs, J.M., Wang, J., Flores-Verdugo, F., Zhang, C., González-Farías, F., 2016. Examining the influence of seasonality, condition, and species composition on mangrove leaf pigment contents and laboratory based spectroscopy data. Rem. Sens. 8, 226. https://doi.org/10.3390/rs8030226.

Flores-de-Santiago, F., Kovacs, J.M., Lafrance, P., 2013. An object-oriented classification method for mapping mangroves in Guinea, West Africa, using multipolarized ALOS PALSAR L-band data. Int. J. Rem. Sens. 34 (2), 563–586. https://doi.org/10.1080/01431161.2012.715773.

Flores-de-Santiago, F., Kovacs, J.M., Flores-Verdugo, F., 2012. Seasonal changes in leaf chlorophyll a content and morphology in a sub-tropical mangrove forest of the Mexican Pacific. Mar. Ecol. Prog. Ser. 444, 57–68. https://doi.org/10.3354/meps09474.

Flores-Verdugo, F., Ramírez-Barrón, E., Flores-de-Santiago, F., 2018. Hydroperiod enhancement using underground pipes for the efficient removal of hypersaline conditions in a semiarid coastal lagoon. Continent. Shelf Res. 162, 39–47. https://doi.org/10.1016/j.csr.2018.04.008.

Flores-Verdugo, F., Zebadua-Penagos, F., Flores-de-Santiago, F., 2015. Assessing the influence of artificially constructed channels in the growth of afforested black mangrove (Avicennia germinans) within an arid coastal region. J. Environ. Manag. 160, 113–120. https://doi.org/10.1016/j.jenvman.2015.06.024.

Flores-Verdugo, F., González-Farías, F., Ramírez-Flores, O., Amezcua-Linares, F., Yáñez-Arancibia, A., Alvarez-Rubio, M., Day, J.W., 1990. Mangrove ecology, aquatic primary productivity, and fish community dynamics in the Teacapán-Agua Brava lagoon-estuarine system (Mexican Pacific). Estuaries 13 (2), 219–230. https://doi.org/10.2307/1351591.

Flores-Verdugo, F.J., Day Jr., J.W., Briseño-Dueñas, R., 1987. Structure, litter fall, decomposition, and detritus dynamics of mangroves in a Mexican coastal lagoon with an ephemeral inlet. Mar. Ecol. Prog. Ser. 35, 83–90. https://doi.org/10.3354/meps035083.

Godwyn-Paulson, P., Jonathan, M.P., Roy, P.D., Rodriguez-Espinosa, P.F., Muthusankar, G., Muñoz-Sevilla, N.P., Lakshumanan, C., 2021. Evolution of southern Mexican Pacific coastline: responses to meteo-oceanographic and physiographic conditions. Regional Studies in Marine Science 47, 101914. https://doi.org/10.1016/j.rsma.2021.101914.

Goldberg, L., Lagomasino, D., Thomas, N., Fatoyinbo, T., 2020. Global decline in human-driven mangrove loss. Global Change Biol. 26, 5844–5855. https://doi.org/10.1111/gcb.15275.

Guo, M., Li, J., Sheng, C., Xu, J., Wu, L., 2017. A review of wetland remote sensing. Sensors 17, 777. https://doi.org/10.3390/s17040777.

Hansen, M.C., Potapov, P.V., Moore, R., Hancher, M., Turubanova, S.A., Tyukavina, A., Thau, D., Stehman, S.V., Goetz, S.J., Loveland, T.R., Kommareddy, A., Egorov, A., Chini, L., Justice, C.O., Townshend, J.R.G., 2013. High-Resolution global maps of 21st-century forest cover change. Science 342, 850–853. https://doi.org/10.1126/science.1244693.

Kamal, M., Sidik, F., Prananda, A.R.A., Mahardhika, S.A., 2021. Mapping leaf area index of restored mangroves using WorldView-2 imagery in perancak estuary, bali, Indonesia. Remote Sens. Appl.: Society and Environment 23, 100567. https://doi.org/10.1016/j.rsase.2021.100567.

Kamal, M., Phinn, S., Johansen, K., 2016. Assessment of multi-resolution image data for mangrove leaf area index mapping. Remote Sens. Environ. 176, 242–254. https://doi.org/10.1016/j.rse.2016.02.013.

Kovacs, J.M., Flores-de-Santiago, F., Bastien, J., Lafrance, P., 2010. An assessment of mangroves in Guinea, West Africa, using a field and remote sensing based approach. Wetlands 30, 773–782. https://doi.org/10.1007/s13157-010-0065-3.

Lassalle, G., Pinheiro Ferreira, M., Cué La Rosa, L.E., Moreira Scafutto, R.D.P., de Souza Filho, C.R., 2023. Advances in multi- and hyperspectral remote sensing of mangrove species: a synthesis and study case on airborne and multisource spaceborne imagery. ISPRS J. Photogrammetry Remote Sens. 195, 298–312. https://doi.org/10.1016/j.isprsjprs.2022.12.003.

Lassalle, G., Ferreira, M.P., La Rosa, L.E.C., de Souza Filho, C.R., 2022. Deep learning-based individual tree crown delineation in mangrove forests using very-high-resolution satellite data. ISPRS J. Photogrammetry Remote Sens. 189, 220–235. https://doi.org/10.1016/j.isprsjprs.2022.05.002.

Li, H., Jia, M., Zhang, R., Ren, Y., Wen, X., 2019. Incorporating the plant phenological trajectory into mangrove species mapping with dense time series Sentinel-2 imagery and the Google Earth Engine platform. Rem. Sens. 11, 2479. https://doi.org/10.3390/rs11212479.

Liang, S., Hu, W., Liu, J., Su, S., Chen, G., Chen, S., Xie, B., Du, J., Liu, W., Chen, B., 2023. Mapping mangrove sustainability in the face of sea level rise and land use: a case study on Leizhou Peninsula, China. J. Environ. Manag. 325, 116554 https://doi.org/10.1016/j.jenvman.2022.116554.

Mafi-Gholami, D., Zenner, E.K., Jaafari, A., 2020. Mangrove regional feedback to sea level rise and drought intensity at the end of the 21st century. Ecol. Indicat. 110, 105972 https://doi.org/10.1016/j.ecolind.2019.105972.

Mahmud, S., Redowan, M., Ahmed, R., Khan, A.A., Rahman, M.M., 2022. Phenology-based classification of Sentinel-2 data to detect coastal mangroves. Geocarto Int. https://doi.org/10.1080/10106049.2022.2087754.

Maurya, K., Mahajan, S., Chaube, N., 2021. Remote sensing techniques: mapping and monitoring of mangrove ecosystem-a review. Complex & Intelligent Systems 7, 2797–2818. https://doi.org/10.1007/s40747-021-00457-z.

Minervino Amodio, A., Di Paola, G., Rosskopf, C.M., 2022. Monitoring coastal vulnerability by using DEMs based on UAV spatial data. ISPRS Int. J. Geo-Inf. 11, 155. https://doi.org/10.3390/ijgi11030155.

Mondal, P., Trzaska, S., de Sherbinin, A., 2018. Landsat-derived estimates of mangrove extents in the Sierra Leone coastal landscape complex during 1990-2016. Sensors 18, 12. https://doi.org/10.3390/s18010012.

Monroy-Torres, M., Flores-Verdugo, F., Flores-de-Santiago, F., 2014. Growth of three subtropical mangrove species in response to varying hydroperiod in an experimental tank. Cienc. Mar. 40 (4), 263–275. https://doi.org/10.7773/cm.v40i4.2455.

Muro-Torres, V., Amezcua, F., Ramírez-Ortiz, G., Flores-de-Santiago, F., Amezcua-Linares, F., Hernández, Y., 2022. Assessing the spatiotemporal relationship between coastal hábitats and fish assemblages at two neotropical estuaries of the Mexican Pacific. Diversity 14, 619. https://doi.org/10.3390/d14080619.

Nagarajan, P., Rajendran, L., Pillai, N.D., Lakshmanan, G., 2022. Comparison of machine learning algorithms for mangrove species identification in Malad creek, Mumbai using WorlView-2 and Google Earth images. J. Coast Conserv. 26, 44. https://doi.org/10.1007/s11852-022-00891-2.

Nguyen, H.H., Nguyen, C.T., Vo, N.D., 2022. Spatial-temporal dynamics of mangrove extent in quang ninh province over 33 years (1987-2020): implications toward mangrove management in vietnam. Regional Studies in Marine Science 52, 102212. https://doi.org/10.1016/j.rsma.2022.102212.

Pham, T.D., Xia, J., Ha, N.T., Bui, D.T., Le, N.N., Tekeuchi, W., 2019. A review of remote sensing approaches for monitoring blue carbon ecosystems: mangroves, seagrasses and salt marshes during 2010-2018. Sensors 19, 1933. https://doi.org/10.3390/s19081933.

Pimple, U., Simonetti, D., Sitthi, A., Pungkul, S., Leadprathom, K., Skupek, H., Som-ard, J., Gond, V., Towprayoon, S., 2018. Google Earth Engine based three decadal Landsat imagery analysis for mapping of mangrove forests and its surroundings in the Trat Province of Thailand. J. Comput. Commun. 6, 247–264. https://doi.org/10.4236/jcc.2018.61025.

Rioja-Nieto, R., Barrera-Falcón, E., Torres-Irineo, E., Mendoza-González, G., Cuervo-Robayo, A.P., 2017. Environmental drivers of decadal change of mangrove forest in the North coast of the Yucatan peninsula, Mexico. J. Coast Conserv. 21, 167–175. https://doi.org/10.1007/s11852-016-0486-0.

Saenger, P., 2002. Mangrove Ecology, Silviculture and Conservation. Klumer Academic Publishers, Dordrecht, p. 360. https://doi.org/10.1007/978-94-015-9962-7.

SAGARPA (Secretaría de Agricultura, Ganadería, Desarrollo Rural, Pesca y Alimentación), 2018. 6to informe de labores 2017-2018. Ciudad de México, p. 168.

Salum, R.B., Souza-Filho, P.W.M., Simard, M., Silva, C.A., Fernandes, M.E.B., Cougo, M.F., Junior, W.d.N., Rogers, K., 2020. Improving mangrove above-ground biomass estimates using LiDAR. Estuar. Coast Shelf Sci. 236, 106585 https://doi.org/10.1016/j.ecss.2020.106585.

Serrano, D., Valle-Levinson, A., 2021. Effects of river discharge and the California Curren ton pycnocline depth at the eastern entrance of the Gulf of California. Continent. Shelf Res. 215, 104356 https://doi.org/10.1016/j.csr.2021.104356.

Schmitt, K., Duke, N.C., 2015. Mangrove management, assessment and monitoring. In: Köhl, M., Pancel, L. (Eds.), Tropical Forestry Handbook. Springer, Berlin, Heidelberg. https://doi.org/10.1007/978-3-642-41554-8_126-1.

Shih, S.S., Huang, Z.Z., Hsu, Y.W., 2022. Nature-based solutions on floodplain restoration with coupled propagule dispersal simulation and stepping-stone approach to predict mangrove encroachment in an estuary. Sci. Total Environ. 851, 158097 https://doi.org/10.1016/j.scitotenv.2022.158097.

Tran, T.V., Reef, R., Zhu, X., 2022. A review of spectral indices for mangrove remote sensing. Rem. Sens. 14, 4868. https://doi.org/10.3390/rs14194868.

Valderrama-Landeros, L., Flores-Verdugo, F., Flores-de-Santiago, F., 2022. Assessing the coastal vulnerability by combining field surveys and the analytical potential of CoastSat in a highly impacted tourist destination. Geographies 2, 642–656. https://doi.org/10.3390/geographies2040039.

Valderrama-Landeros, L., Flores-Verdugo, F., Rodríguez-Sobreyra, R., Kovacs, J.M., Flores-de-Santiago, F., 2021. Extrapolating canopy phenology information using Sentinel-2 data and the Google Earth Engine platform to identify the optimal dates for remotely sensed image acquisition of semiarid mangroves. J. Environ. Manag. 279, 111617 https://doi.org/10.1016/j.jenvman.2020.111617.

Valderrama-Landeros, L., Blanco y Correa, M., Flores-Verdugo, F., Álvarez-Sánchez, L.F., Flores-de-Santiago, F., 2020. Spatiotemporal shoreline dynamics of Marismas Nacionales, Pacific coast of Mexico, based on a remote sensing and GIS mapping approach. Environ. Monit. Assess. 192, 123. https://doi.org/10.1007/s10661-020-8094-8.

Valderrama-Landeros, L., Flores-de-Santiago, F., 2019. Assessing coastal erosion and accretion trends along two contrasting subtropical rivers based on remote sensing data. Ocean Coast Manag. 169, 58–67. https://doi.org/10.1016/j.ocecoaman.2018.12.006.

Valderrama-Landeros, L., Flores-de-Santiago, F., Kovacs, J.M., Flores-Verdugo, F., 2018. An assessment of commonly employed satellite-based remote sensors for mapping mangrove species in Mexico using an NDVI-based classification scheme. Environ. Monit. Assess. 190 (23), 1–12. https://doi.org/10.1007/s10661-017-6399-z.

Vizcaya-Martínez, D.A., Flores-de-Santiago, F., Valderrama-Landeros, L., Serrano, D., Rodríguez-Sobreyra, R., Álvarez-Sánchez, L.F., Flores-Verdugo, F., 2022. Monitoring detailed mangrove hurricane damage and early recovery using multisource remote sensing data. J. Environ. Manag. 320, 115830 https://doi.org/10.1016/j.jenvman.2022.115830.

Vundavilli, H., Mullarney, J.C., MacDonald, I.T., Bryan, K.R., 2021. The interaction of buoyant coastal river plumes with mangrove vegetation and consequences for sediment deposition and erosion in a tidal environment. Continent. Shelf Res. 222, 104417 https://doi.org/10.1016/j.csr.2021.104417.

Wang, H., Peng, Y., Wang, C., Wen, Q., Xu, J., Hu, Z., Jia, X., Zhao, X., Lian, W., Temmerman, S., Wolf, J., Bouma, T., 2021. Mangrove loss and gain in a densely populated urban estuary: lessons from the Guangdong-Hong Kong-Macao Greater Bay area. Front. Mar. Sci. 8, 693450 https://doi.org/10.3389/fmars.2021.693450.

Wang, D., Wan, B., Qiu, P., Zuo, Z., Wang, R., Wu, X., 2019. Mapping height and aboveground biomass of mangrove forests on Hainan Island using UAV-LiDAR sampling. Rem. Sens. 11, 2156. https://doi.org/10.3390/rs11182156.

Wang, M., Cao, W., Guan, Q., Wu, G., Wang, F., 2018. Assessing changes of mangrove forest in a coastal region of southeast China using multi-temporal satellite images. Estuar. Coast Shelf Sci. 207, 283–292. https://doi.org/10.1016/j.ecss.2018.04.021.

Zambrano-Medina, Y., Franco-Ochoa, C., Plata-Rocha, W., García-Páez, F., Montoya-Rodríguez, M., Mendoza-Baldwin, E., 2022. Shoreline análisis and erosión risk assessment of a coastal strip subjected to high anthropogenic pressure. Tecnología y Ciencias del Agua 13 (6), 249–300. https://doi.org/10.24850/j-tyca-13-06-06.

Zhang, Z., Xu, N., Li, Y., Li, Y., 2022. Sub-continental -scale mapping of tidal wetland composition for East Asia: a novel algorithm integrating satellite tide-level and phenological features. Remote Sens. Environ. 269, 112799 https://doi.org/10.1016/j.rse.2021.112799.

Zhen, J., Jiang, X., Xu, Y., Miao, J., Zhao, D., Wang, J., Wang, J., Wu, G., 2021. Mapping leaf chlorophyll content of mangrove forests with Sentinel-2 images of four periods. Int. J. Appl. Earth Obs. Geoinf. 102, 102387 https://doi.org/10.1016/j.jag.2021.102387.